Tetrahedron 66 (2010) 8446–8449

Contents lists available at ScienceDirect

Tetrahedron

journal homepage: www.elsevier.com/locate/tet

^{31}P NMR kinetic study of the tandem cleavage of phosphonate esters by bromotrimethylsilane

Anne C. Conibear, Kevin A. Lobb, Perry T. Kaye *

Department of Chemistry and Centre for Chemico- and Biomedicinal Research, Rhodes University, Grahamstown 6140, South Africa

ARTICLE INFO

Article history:
Received 27 May 2010
Received in revised form
4 August 2010
Accepted 23 August 2010
Available online 27 August 2010

Keywords:
Phosphorus-31 NMR
Phosphonate esters
Kinetics
Bromotrimethylsilane

ABSTRACT

^{1}H and ^{31}P NMR methods have been used to access rate constants and activation parameters for each of the consecutive second-order silylation reactions involved in the overall transformation (**1a**→**3a**→**4a**), while computational optimisation of the rate constants obtained from the initial, linear phase of each reaction has permitted an excellent fit with the experimental data for the entire course of the reaction.

1. Introduction

1-Deoxy-D-xylulose-5-phosphate-reductoisomerase (DXR) plays an essential role in the parasite-specific, *Plasmodium falciparum* (*Pf*) isoprenoid biosynthetic pathway.[1] Fosmidomycin and FR900098[2] have been shown to inhibit DXR, and we have been exploring the development of novel analogues as competitive DXR-inhibitors and, hence, as potential antimalarial agents. Particular attention has been focused on the synthesis of the phosphonated *N*-heteroarylalkanamides **1a**–**e** and **2a**–**e** (Scheme 1)[3] and their *N*-phenyl analogues.[4] Various approaches to the critical hydrolysis step (**1**→**2**) have been reported, including tandem trimethylsilylation [using bromotrimethylsilane (TMSBr)] and hydrolysis,[5,6] and we have successfully used Kumar's microwave-assisted method[5] for the 'hydrolysis' of a series of diethyl [*N*-(phenyl)carbamoyl]-methylphosphonates[4] to the corresponding phosphonic acids. However, attempts to hydrolyse the *N*-heteroaryl analogues **1b**, **1c** and **1d** using this method were unsuccessful and, although application of a modification of Geissmann's method[6] proved successful, the reaction time required was considerably longer than predicted.

In order to elucidate and, perhaps, optimise the transformation, we decided to explore the kinetics of the consecutive silylation reactions leading to the formation of the bis(trimethylsilyl) ester **4a** from the phosphonate ester **1a** (Scheme 2); on treatment with water, the former is readily converted to the desired phosphonic

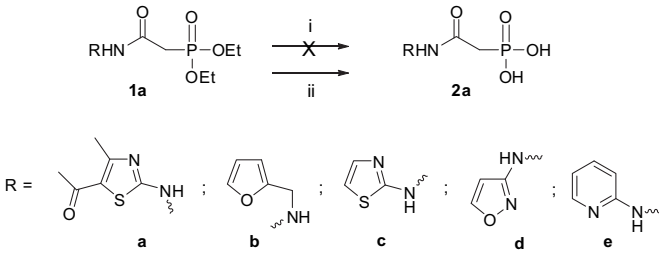

Scheme 1. Reagents and conditions (i) CH_3CN, TMSBr (2 equiv), μW (100 W; 60 °C; 10 min), then 95:5 MeOH/H_2O. (ii) TMSBr (4 equiv, DCM, N_2, overnight, then 0.4M-NaOH.

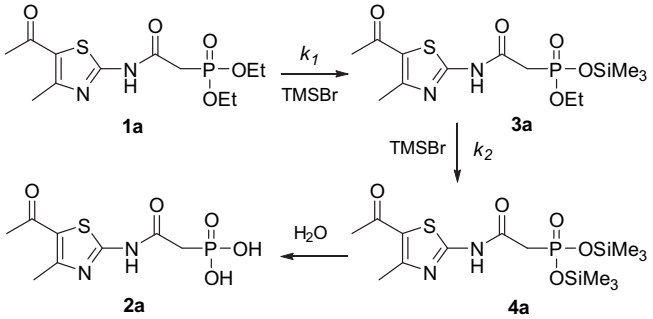

Scheme 2. Overall transformation analysed in the kinetic study.

* Corresponding author. Tel.: +27 46 6037030; fax: +27 466225109; e-mail address: P.Kaye@ru.ac.za (P.T. Kaye).

0040-4020/$ – see front matter © 2010 Elsevier Ltd. All rights reserved.
doi:10.1016/j.tet.2010.08.058

acid **2a**. The use of TMSBr to form bis(trimethysilyl) esters was introduced by McKenna et al.,[7] who monitored the progress of the reaction by ^{1}H and ^{31}P NMR spectroscopy but did not, it seems, undertake a detailed kinetic study. In this communication, we now discuss the results of a kinetic study, which has:—(i) involved the use of ^{1}H and ^{31}P NMR spectroscopy; (ii) provided rate constants and activation parameters for each of the consecutive reactions; and (iii) illustrated the use of two methods for the analysis of consecutive second-order kinetic data, which do not require equimolar amounts of the starting materials or pseudo first-order conditions.

2. Results and discussion

The conversion of the diethyl phosphonates **1** to the bis(trimethylsilyl)phosphonates **4** involves the replacement of two ethyl groups by two trimethylsilyl groups, and is presumed[7] to follow a mechanism (Scheme 3) similar to that of the Arbuzov reaction. ^{1}H and ^{31}P NMR spectra were obtained for solutions of the substrate **1a** in dry $CDCl_3$ at 90 s intervals during the course of the reaction, and the concentrations of the three phosphorus-containing species (**1a**, **3a** and **4a**) were determined from the relative integral data. The ^{31}P T_1 relaxation time for each of these species was measured to ensure that the recycle (acquisition+delay) time used (2.9 s) permitted complete relaxation of the phosphorus nuclei and, hence, that the integral data are proportional to their relative concentrations. The changes in the concentration of TMSBr were determined from the corresponding ^{1}H NMR spectra, using 1,3,5-trimethoxybenzene (TMB) as an internal standard. Inverse-gated proton decoupling was also used. The ^{31}P T_1 relaxation times (ms) and ^{31}P chemical shift values (δ/ppm relative to the phosphoric acid standard) for the three phosphorus-containing species were:—**1a**: 536 and 19.19; **3a**: 542 and 9.37 and **4a**: 553 and −0.69. It is apparent, from the ^{31}P spectra illustrated in the stack-plot (Fig. 1), that the signals for the three ^{31}P nuclei are well resolved as replacement of the ethyl groups by trimethylsilyl groups is accompanied by progressive shielding of the ^{31}P nuclei.

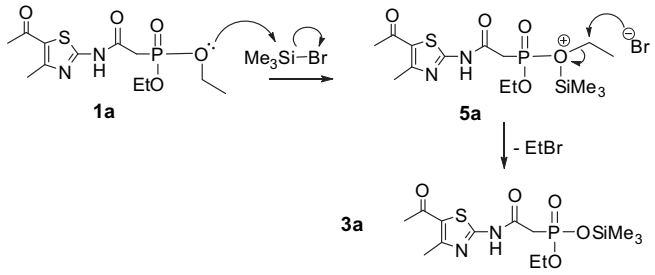

Scheme 3. Putative mechanism for the reaction (step 1) of the phosphonate diester **1a** with trimethylsilyl bromide, following McKenna's proposal.[7]

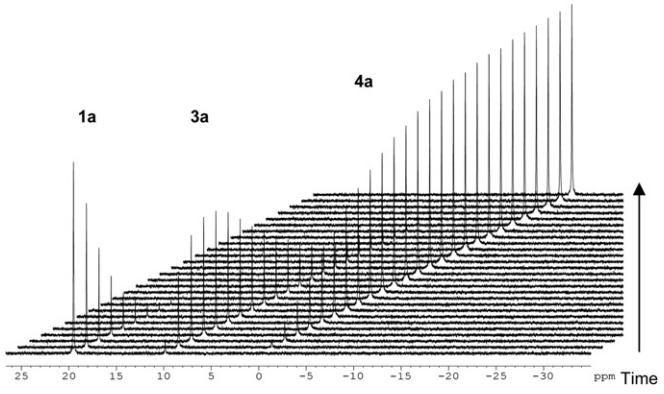

Fig. 1. Stack-plot illustrating ^{31}P NMR signals for starting material **1a**, intermediate **3a** and product **4a** at 285 K, at 30 min intervals.

A plot of the concentrations of the starting material **1a** and the mono- and disilylated derivatives (**3a** and **4a**, respectively) against time (Fig. 2) reveals curves that are typical of a two-step reaction in which $k_1 \approx k_2$.[8] As expected, the curve for the formation of the product **4a** is sigmoidal in shape and has a point of inflexion at the time corresponding to $[\mathbf{3a}]_{max}$; the delay in the appearance of the product **4a** (which is responsible for the sigmoidal curve) implies involvement of an intermediate in the reaction.[8]

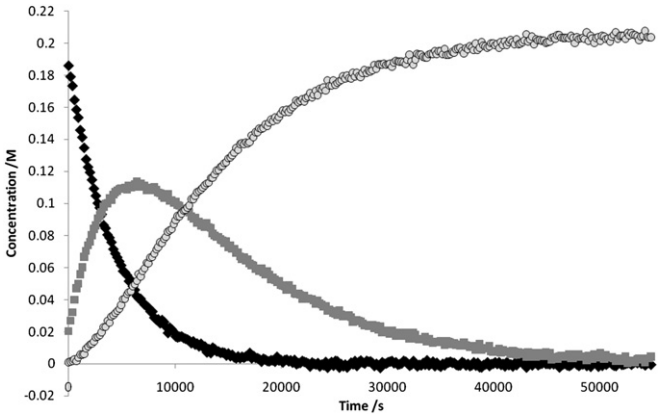

Fig. 2. Graph of concentration against time for the reaction of phosphonate ester **1a** with TMSBr at 283 K, showing the three phosphorus-containing species: starting material **1a** as black diamonds, intermediate **3a** as grey squares and product **4a** as light grey circles.

Analysis of the first step, involving consumption of the starting material **1a**, indicated that it follows second-order rather than the simple first-order kinetics used in the treatment provided by Schmid and Sapunov.[8] Consequently, the possibility of establishing pseudo first-order conditions was explored by using 32 equiv of TMSBr. Under these conditions, however, the ^{31}P signals broadened significantly and changes in the chemical shift values were noted. In order to avoid unnecessary complications (involving, perhaps, the formation of polysilylated products, such as compound **6**[9]) the well-resolved, second-order data were used.

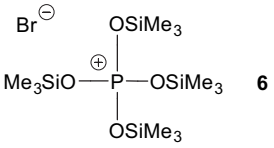

6

Frost and Schwemer,[10] have integrated the differential rate equations for competitive consecutive second-order reactions based on very similar transformations, *viz*., the saponification of ethyl adipate and ethyl succinate, and their treatment has been extended into a computer programme by Burkhard.[11] Unfortunately, these approaches only apply to the use of stoichiometrically equivalent quantities of the two reactants. Our analysis of the reaction between the phosphonate ester **1a** and TMSBr, on the other hand, is based on a consideration of two, separate, second-order reactions of the general form: $A+B \rightarrow P$. The rate of such a reaction is given by Eq. 1 in which k is the corresponding second-order rate constant:

$$\frac{-\mathrm{d}[A]}{\mathrm{d}t} = k[A][B] \qquad (1)$$

When the starting concentrations $[A]_0$ and $[B]_0$ of the two reactants are different, the variable x is used such that $[A]_0 - x = [A]$ and $[B] - x = [B]_0$, and Eq. 1 becomes:

$$\frac{dx}{([A]_0-x)([B]_0-x)} = kdt \quad (2)$$

After partial fraction expansion and integration, Eq. 2 becomes:

$$\frac{1}{[B]_0-[A]_0}\ln\frac{[A]_0-x}{[B]_0-x} = kt + C \quad (3)$$

where $C = \frac{1}{[B]_0-[A]_0}\ln\frac{[A]_0}{[B]_0}$ when x=0 and t=0

$$\ln\frac{[B]_0[A]}{[A]_0[B]} = kt([B]_0-[A]_0) \quad (4)$$

As the reactant concentrations [A] and [B] can be measured using the NMR integral data, Eq. 4 (developed by Keusch),[12] was used to calculate the rate constants, k_1 and k_2 for the first and second steps, respectively. For the first step, $[A]_0$=initial concentration of the substrate **1a**, while $[B]_0$=initial concentration of TMSBr. $\ln([B]_0[A]/[A]_0[B])$ was plotted against time and the gradient for the initial, linear portion of the graph was divided by $([B]_0-[A]_0)$ to afford the rate constant k_1 for the first step (**1a**→**3a**). The second-order component of the second step (**3a**→**4a**) occurs upon complete consumption of the substrate **1a**, at which stage the only reaction occurring involves conversion of the monosilylated intermediate **3a** to the product **4a**. At this point, $[A]_0$=[**3a**] and $[B]_0$=[TMSBr] and Eq. 4 was again used to determine the second-order rate constant for the second step, k_2. The linearity of the second-order kinetic plots confirms that both steps are second-order—observations, which are consistent with the mechanism proposed by McKenna (Scheme 3).[7]

Reactions were conducted at various temperatures between 283 and 303 K and Arrhenius plots (R^2=0.9547 and 0.8904, respectively) for the first (**1a**→**3a**) and second steps (**3a**→**4a**) permitted evaluation of the respective activation energies E_a (Table 1) and an Eyring plot[13] (R^2=0.9553 and 0.8792, respectively) permitted direct evaluation of the activation parameters $\Delta H^{\ddagger}$ and $\Delta S^{\ddagger}$ and, thence, $\Delta G^{\ddagger}$ at 298.15 K.

Table 1
Kinetic parameters of the reaction between **1a** and TMSBr determined using the initial, linear portions of the experimental data

Parameter	Calculated values[a]/kcal mol^{-1}	
	Step 1	Step 2
E_a	11.63±0.80	10.7±1.4
$\Delta H^{\ddagger}$	10.29±0.74	10.1±1.4
$\Delta S^{\ddagger}$	−38.9±2.5[b]	−41.8±4.8[b]
$\Delta G^{\ddagger}$	21.9±1.5	22.5±1.6

[a] Uncertainties were calculated from the respective standard errors for the slope and intercept for each graph.
[b] Cal K^{-1} mol^{-1}.

A computational method was then employed to refine the estimates of the activation parameters obtained using Eq. 4 and thus improve the correlation with the experimental data. Using the previously calculated values of k_1 and k_2 as initial estimates, the concentrations of each of the species **1a**, **3a** and **4a** were predicted at 1 s intervals from the second-order rate equation (Eq. 1). Building on a method used in earlier work,[14] k_1 and k_2 were varied independently within a range of their initial values.[15] For each experiment, graphs were plotted comparing the experimental data with:—(a) the original k_1 and k_2 values, obtained using Eq. 4; and (b) the computationally optimised k_1 and k_2 values. The improved fit obtained with the latter values is illustrated in Fig. 3. The linearity of both the Arrhenius (R^2=0.9673 and 0.9620, respectively) and Eyring plots (R^2=0.9738 and 0.9686, respectively) is also improved (the latter illustrated in Fig. 4), thus affording activation parameters (Table 2) with smaller uncertainty values—particularly for the second step of the reaction. As expected for a bimolecular reaction, $\Delta S^{\ddagger}$ is negative due to the accompanying decrease in entropy in each case.

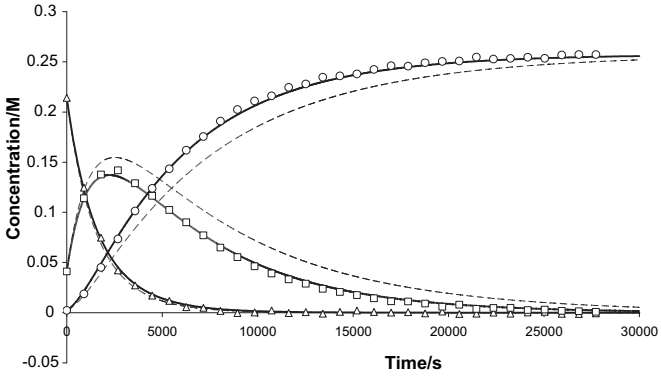

Fig. 3. Plots of concentration against time for the reaction of phosphonate ester **1a** with TMSBr at 297 K, showing the three phosphorus-containing species: starting material **1a** as open triangles, intermediate **3a** as open squares and product **4a** as open circles. The fit of the experimental data with the values of k_1 and k_2 obtained from Eq. 4 is shown by dashed lines. The significantly improved fit of the experimental data with the computationally optimised k_1 and k_2 values is shown by solid lines. For clarity, only a limited number of points are plotted for each curve.

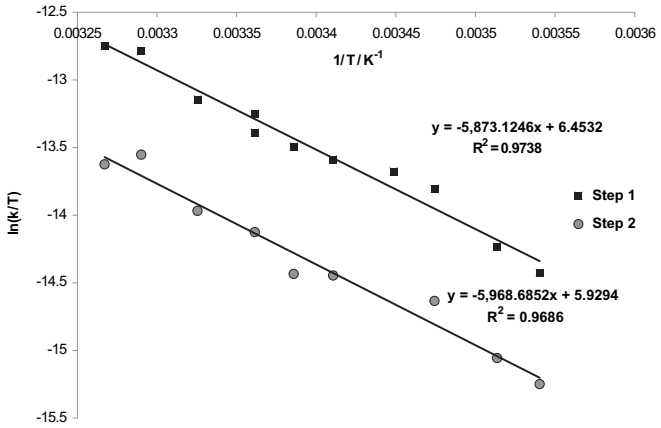

Fig. 4. Eyring plots of $\ln(k/T)$ against $1/T/K^{-1}$ for step 1 (shown in black squares) and step 2 (shown in grey circles) for the reaction between **1a** and TMSBr using computationally optimised k_1 and k_2 values.

Table 2
Kinetic parameters of the reaction between **1a** and TMSBr calculated[a] using computationally optimised k_1 and k_2 values

Parameter	Calculated values[a]/kcal mol^{-1}	
	Step 1	Step 2
E_a	13.07±0.76	12.44±0.81
$\Delta H^{\ddagger}$	11.67±0.64	11.86±0.81
$\Delta S^{\ddagger}$	−34.4±2.2[b]	−35.4±2.7[b]
$\Delta G^{\ddagger}$	21.9±1.3	22.4±1.6

[a] Uncertainties were calculated from the respective standard errors for the slope and intercept for each graph.
[b] Cal K^{-1} mol^{-1}.

3. Conclusions

Second-order analysis of both steps of the overall transformation (**1a**→**3a**→**4a**) clearly provides an accurate description of the process and supports the mechanism proposed by McKenna[7] (Scheme 3). While the initial estimates of k_1 and k_2 correlate well with the experimental data over the initial, linear phase of each

reaction (**1a**→**3a** and **3a**→**4a**), the computationally optimised values of k_1 and k_2 provide a far better fit with the experimental data over the whole course of the reaction. Analysis of the second-order kinetic data has thus afforded access to rate constants and activation parameters for each of the consecutive reactions without recourse to either pseudo first-order conditions or the use of equimolar quantities of the starting materials. The study has also highlighted the usefulness of ^{31}P NMR spectroscopy for kinetic studies with the concomitant advantages of uncluttered spectra and short relaxation times facilitating accurate determination of the concentrations of the species involved.

4. Experimental

4.1. General

The study was conducted using a Bruker Biospin 600 MHz spectrometer, and temperature calibration of the probe was carried out following standard procedures.[16,17] The preparation and characterisation of the phosphonate ester **1a** and the corresponding phosphonic acid **2a** are described elsewhere.[3]

4.2. Measurement of the ^{31}P T_1 relaxation times

Diethyl phosphonate **1a** (0.060 g, 0.18 mmol) and 1,3,5-trimethoxybenzene (TMB; 0.012 g, 0.068 mmol) were dissolved in dry $CDCl_3$ (0.6 mL; stored over molecular sieves and basic alumina) under N_2. The solution was transferred to an NMR tube, which was then flushed with N_2 and sealed with a septum. The ^{1}H and ^{31}P NMR spectra [calibrated relative to 1M-phosphoric acid in D_2O (0.00 ppm)] of the substrate **1a** and TMB were recorded and 1 equiv of TMSBr (0.024 mL, 0.18 mmol) was then added through the septum. The reaction mixture was shaken and left to stand overnight at room temperature. The T_1 relaxation times of the phosphorus nuclei (in **1a**, **3a** and **4a**) were measured by recording the inversion recovery ^{31}P spectra in a series of 12 experiments involving different recovery times ranging from 100 ms to 20 s. The ^{31}P signals were integrated and the intensity plotted against the delay time to give the T_1 relaxation times.

4.3. Kinetics of the reaction of 1a with TMSBr

For each kinetic run, weighed quantities of the substrate **1a** and TMB were dissolved in dry $CDCl_3$ (0.6 mL; stored over molecular sieves and basic alumina) under N_2. The solution was transferred to a graduated NMR tube, flushed with N_2 and sealed with a septum. The ^{1}H and ^{31}P spectra of the substrate solution were recorded and TMSBr (4 equiv) was then added. The total volume of the reaction mixture was recorded and the tube was immediately replaced in the probe. The NMR experiments were set to record both the ^{1}H and ^{31}P spectra, followed by a delay of 90 s between acquisitions. The experiments were repeated at different temperatures ranging from 283 to 305 K.

4.4. Preparation of bis(trimethylsilyl) 2-[(5-acetyl-4-methyl-1,3-thiazol-2-yl)-carbamoyl]ethylphosphonate 4a

As the bis(trimethylsilyl) phosphonate **4a** readily hydrolyses on contact with air, it was synthesised in an NMR tube and characterised in the reaction mixture in the presence of the by-product, ethyl bromide, excess TMSBr and TMB. A solution of the diethyl phosphonate **1a** (0.060 g, 0.18 mmol) and TMB (0.010 g, 0.060 mmol) in dry $CDCl_3$ under N_2 was transferred to an NMR tube, which was flushed with N_2 and sealed with a septum. TMSBr (0.095 mL, 0.72 mmol) was added through the septum and the reaction monitored by ^{1}H and ^{31}P NMR spectroscopy until the conversion **1a**→**4a** was complete. Spectroscopic data for compound **4a** were as follows: δ_H (600 MHz; $CDCl_3$) −0.03 (18H, s, 6×CH_3Si), 2.48 (3H, s, CH_3), 2.66 (3H, s, CH_3C═O), 3.45 (2H, d, J=22.8 Hz, CH_2P); δ_C (150 MHz; $CDCl_3$) 1.7 (q, 6×CH_3Si), 15.4 (q, CH_3C═O), 29.9 (q, CH_3), 38.4 (d, J_{C-P}=136.5 Hz, CH_2P), 125.4 (s, C-4), 160.4 (s, C-5), 161.3 (s, C-2), 164.4 (s, NHC═O), 189.0 (s, CH_3C═O); δ_P (243 MHz; $CDCl_3$) −0.69.

Acknowledgements

The authors thank the Beit Trust for a bursary (to A.C.C.), Rhodes University, the South African Medical Research Council (MRC) and the National Research Foundation (NRF: GUN 2069255) for generous financial support, and Professor M. E. Brown for helpful advice. Any opinion, findings and conclusions or recommendations expressed in this material are those of the authors and therefore the NRF does not accept any liability in regard thereto.

Supplementary data

Supplementary spectroscopic data associated with this article can be found in the online version at doi:10.1016/j.tet.2010.08.058.

References and notes

1. Rohmer, M.; Seemann, M.; Horbach, S.; Bringer-Meyer, S.; Sahm, H. *J. Am. Chem. Soc.* **1996**, *118*, 2564–2566.
2. Jomaa, H.; Wiesner, J.; Sanderbrand, S.; Altincicek, B.; Weidemeyer, C.; Hintz, M.; Türbachova, I.; Eberl, M.; Zeidler, J.; Lichtenthaler, H. K.; Soldati, D.; Beck, E. *Science* **1999**, *285*, 1573–1576.
3. Conibear, A.C. M.Sc thesis, Rhodes University, 2010.
4. Mutorwa, M.; Salisu, S.; Blatch, G. L.; Kenyon, C.; Kaye, P. T. *Synth. Commun.* **2009**, *39*, 2723–2736.
5. Kumar, K. G. D.; Saenz, D.; Lokesh, G. L.; Natarajan, A. *Tetrahedron Lett.* **2006**, *47*, 6281–6284.
6. Giessmann, D.; Heidler, P.; Haemers, T.; Van Calenbergh, S.; Reichenberg, A.; Jomaa, H.; Weidemeyer, C.; Sanderbrand, S.; Wiesner, J.; Link, A. *Chem. Biodiversity* **2008**, *5*, 643–656.
7. McKenna, C. E.; Higa, M. T.; Cheung, N. H.; McKenna, M. *Tetrahedron Lett.* **1977**, *18*, 155–158.
8. Schmid, R.; Sapunov, V. N. General Reaction Types; In *Non-formal Kinetics*; Dyllick-Brenzinger, C., Ed.; Verlag Chemie: Weinheim, 1982; Vol. 14, pp 14–19.
9. Schmidbaur, H.; Seeber, R. *Chem. Ber.* **1974**, *107*, 1731–1738; (CA 1974:449746).
10. Frost, A. A.; Schwemer, W. C. *J. Am. Chem. Soc.* **1952**, *74*, 1268–1273.
11. Burkhard, C. A. *Ind. Eng. Chem.* **1960**, *52*, 678.
12. Keusch, P. Chemical Kinetics Rate Laws, Arrhenius Equation—Experiments. http://www.uni-regensburg.de/Fakultaeten/nat_Fak_IV/Organische_Chemie/Didaktik/Keusch/kinetics.htm (accessed 07/20/2009).
13. Laidler, K. J.; King, M. C. *J. Phys. Chem.* **1983**, *87*, 2657–2664.
14. Kaye, P. T.; Mphahlele, M. J.; Brown, M. E. *J. Chem. Soc., Perkin Trans. 2* **1995**, 835–838.
15. For each pair of k_1 and k_2 values, the resultant curve of the calculated concentrations was compared with the experimental values and an R^2 value was calculated. The values of k_1 and k_2 giving the minimum R^2 value were readily identified and appeared to provide the best fit with the Experimental data. These calculations were carried out using the computer programme available as Supplementary data. (K. Lobb, 2010).
16. Nicholls, A. W.; Mortishire-Smith, R. J. *Magn. Reson. Chem.* **2001**, *39*, 773–776.
17. Van Geet, A. L. *Anal. Chem.* **1968**, *40*, 2227–2229.